Carbon reaction and diffusion on Ni(111), Ni(100), and Fe(110): Kinetic parameters from x-ray photoelectron spectroscopy and density functional theory analysis

A. Wiltner,[1] Ch. Linsmeier,[1,a)] and T. Jacob[2]
[1]*Max-Planck-Institut für Plasmaphysik, EURATOM Association, Boltzmannstrasse 2, D-85748 Garching b. München, Germany*
[2]*Fritz-Haber-Institut der Max-Planck-Gesellschaft, Faradayweg 4-6, D-14195 Berlin, Germany*

(Received 20 February 2008; accepted 22 July 2008; published online 25 August 2008)

This paper investigates the reactivity of elemental carbon films deposited from the vapor phase with Fe and Ni substrates at room temperature. X-ray photoelectron spectroscopy (XPS) measurements are presented as a method for evaluating kinetic reaction data. Carbon films are deposited on different surface orientations representing geometries from a dense atom packing as in fcc (111) to an open surface structure as in fcc (100). During annealing experiments several reactions are observed (carbon subsurface diffusion, carbide formation, carbide decomposition, and graphite ordering). These reactions and the respective kinetic parameters are analyzed and quantified by XPS measurements performed while annealing at elevated temperatures (620–820 K). The resulting activation barriers for carbon subsurface diffusion are compared with calculated values using the density functional theory. The determined kinetic parameters are used to reproduce the thermal behavior of carbon films on nickel surfaces. © *2008 American Institute of Physics*.
[DOI: 10.1063/1.2971177]

I. INTRODUCTION

The investigation of diffusion and segregation as well as the determination of kinetic parameters of carbon in Fe and Ni are reported in literature by several authors. The resulting activation barriers differ strongly. Most diffusion barriers given in the literature are determined as bulk values. A summary about diffusion barriers and diffusivity of carbon in Fe and Ni is given in Ref. 1. Diamond and Wert[2] analyzed the carbon diffusion by the anelastic behavior of C dissolved in Ni and determined an activation barrier of 1.5 eV between 370 and 800 K. Massaro and Petersen[3] investigated ^{14}C films after ethylene decomposition on polycrystalline Ni samples and determined a smaller diffusion barrier of 0.87 eV between 620 and 970 K. In a short comment Berry[4] confronted this value with 1.73 eV, determined above 970 K, and suggested one activation barrier applicable at all temperatures. This assumption is in agreement with density functional theory (DFT) calculations by Siegel and Hamilton.[5] The authors calculated the bulk diffusion barrier for carbon migration along octahedral sites (1.75 eV) and along octahedral via tetrahedral sites (1.62 eV). The latter value seemed to be more favorable. In addition, they determined different heats of solution for carbon in paramagnetic and ferromagnetic nickel (Curie temperature T_C=627 K). Diamond and Wert[2] observed in their first measurements a negligible effect of the magnetic state on the diffusion barrier. The values given above represent activation barriers for carbon diffusion in bulk material. Schouten *et al.*[6,7] investigated the carbon dissolution through different Ni planes by Auger electron spectroscopy (AES) measurements. They determined diffusion barriers of 1.54 eV (370–770 K) on Ni(110) and 1.21 eV (474–563 K) on Ni(100). The carbon films were deposited by methane decomposition in the given temperature ranges. On Ni(111) the authors could not deposit carbon films by this procedure. Sau and Hudson[8] deposited carbidic and graphitic carbon films on Ni(110) by ethylene decomposition at temperatures between 575 K (carbidic carbon films) and 775 K (graphitic carbon films) and analyzed them by AES measurements. For graphitic carbon films they determined a diffusion barrier of 3.9 eV above 883 K. At lower temperatures the dissolution process did not follow a first order reaction and an activation barrier was not determined. Moreover, they did not determine a diffusion barrier for the carbidic carbon layer due to slow carbon dissolution. DFT calculations of carbon films on different Ni planes are not reported by now. As mentioned above, the diffusion barriers for carbon dissolution into Ni through different surface planes were determined after hydrocarbon decomposition reactions. In this work we deposit elemental carbon films from the vapor phase while keeping the substrates at room temperature (RT). This facilitates the analysis of carbon diffusion from the surface to subsurface positions (initial step for carbon bulk diffusion) without the need of any additional decomposition reaction.

Carbon diffusion in Fe was reported in the literature by several authors. Due to the rearrangement of the Fe lattice from α-Fe [body-centered cubic (bcc)] to γ-Fe [face-centered cubic (fcc)] at temperatures above 1010 K, different activation barriers are expected.[9] Between 500 and 890 K the diffusion barrier (0.8 eV) follows an Arrhenius behavior, whereas at higher temperatures the linear dependence is no longer observed.[1] McLellan and Wacz[10] summarized the

a)Electronic mail: linsmeier@ipp.mpg.de.

TABLE I. Free energy of formation at 300 K (Ref. 18) for carbides described in Refs. 14–17—Fe_3C and Ni_3C—Refs. 21 and 28.

Carbide	ΔG_f^0 (eV)
TiC	−1.87
Be_2C	−1.19
SiC	−0.73
WC	−0.40
W_2C	−0.23
Fe_3C	+0.21
Ni_3C	+0.66

available experimental values for carbon diffusion in α- and γ-Fe. The average diffusion barrier in α-Fe is determined to 0.84 eV. DFT calculations for carbon bulk diffusion in both lattice structures are in good agreement with these experimental values (0.86 eV for α-Fe).[11] The diffusion barriers given in literature are again bulk values, whereas this work focuses on the surface-subsurface diffusion as the elementary step in C dissolution. Dissolution measurements of carbon films on different Fe planes and a determination of diffusion barriers are not reported to our knowledge. Moreover, DFT calculations considering the Fe surface orientation are not available in the literature.

Carbon films deposited by thermal hydrocarbon or carbon monoxide decomposition on Fe and Ni surfaces are investigated with respect to their use as catalysts (e.g., Ref. 12). A recent review by Hwu *et al.*[13] provided a comprehensive overview of the chemical reactions between transition metal carbide surfaces and a variety of inorganic and organic molecules. In this work we investigate the interaction of elemental carbon films deposited on Fe and Ni surfaces with different surface structures. The formation reaction of the respective carbides (Fe_3C and Ni_3C) are endothermic, in contrast to almost all other carbides. We already studied the thermal behavior of elemental carbon films on W, Ti, Si, and Be.[14–17] These elements form carbides in an exothermic formation reaction. For Ni_3C and Fe_3C, however, the enthalpies of formation are positive, and the formation reaction is therefore endothermic.[18] The respective values of the carbide formation reactions (free energy of formation and Gibbs function ΔG_f^0) are given in Table I. In addition to the reactivities of Fe and Ni with C, the metal and carbide structures have to be taken into account in the discussion of mobilities of species during solid state reactions. Si and Be form carbides with a prominent ionic bond character.[19] In agreement with this, we do not observe a dissolution of the carbon layers into the bulk at high temperatures.[14,17] The carbides, once formed, are stable in their carbon-metal stoichiometries up to 900 K (Be_2C) and 1100 K (SiC), respectively. All other substrates investigated up to now and discussed in this work form metallic (intercalation) carbides with carbon atoms in different sites within the metal lattices. The Ti lattice with a hexagonal close packing (hcp) possesses octahedral sites large enough for carbon atom incorporation. TiC is formed if all octahedral sites are filled by carbon atoms.[20] However, not all available sites are occupied by carbon atoms and therefore stoichiometric TiC (Ti:C=1:1) is not observed in real crystals. The maximum stoichiometric ratio reported in literature is $TiC_{0.95}$.[9] A successive filling of octahedral sites by carbon atoms leads to subcarbides (Ti_xC_y, $y<x$). Both species (TiC and subcarbides) are observed in our experiments.[17] Metallic W has a bulk bcc structure. The octahedral sites within this metal lattice are too small for carbon atom incorporation.[19] Therefore, the metal lattice rearranges during carbide formation. W_2C, tungsten subcarbide, is observed after W rearrangement into a hcp structure with carbon atoms in $\frac{1}{2}$ of octahedral sites.[20] The tungsten carbide, WC, is created by a rearrangement of W into a hexagonal primitive packing with carbon atoms in trigonal prismatic sites.[20] In previous experiments performed in our group, both carbides are observed.[17] W_2C is stable between 1100 and 1300 K, whereas WC is formed above 1300 K. Both in Ti and W binary systems with carbon, the carbide formation starting with layers on the metals is accompanied by carbon diffusion. The incorporation of carbon atoms in sites within the metal lattice requires carbon migration in agreement with this observation. Moreover, the amount of formed carbide agrees with the tendency of the Gibbs free energy for the carbide formation reaction (see Table I). Furthermore, the onset in carbon diffusion complies with the tendency of the respective diffusion barriers (bulk values) for these metals. Ti (1.3 eV) shows the lowest onset temperature, followed by W (1.8 eV).[1]

In the temperature region investigated in this work, Fe has a bcc structure (α-Fe).[9] The octahedral sites are again too small for carbon atom incorporation.[19] During carbide formation, the metal lattice has to rearrange into a orthorhombic structure, in which the carbon atoms occupy trigonal prismaticlike sites.[20,21] In the case of Ni_3C formation, the metal lattice (fcc) rearranges into a hcp structure (similar to W_2C) with carbon atoms in octahedral sites.[20,21] From these structure data, we expect a similar thermal behavior of carbon films on W, Ti, Fe, and Ni. The endothermic carbide formation reactions of Fe_3C and Ni_3C should lead to different carbide amounts after RT deposition and in annealing experiments.

Experimentally, we select x-ray photoelectron spectroscopy (XPS) analysis using monochromatic Al $K\alpha$ radiation and carry out carbon deposition with thicknesses from submonolayer to several nanometers. The high surface sensitivity of XPS with information depths of several nanometers allows us to perform chemical state analysis from the film surface, the film-substrate interface, to the first substrate layers. Therefore, XPS promises a detailed examination of the surface reaction steps and analysis of the influence of the surface orientation on them.

II. METHODS

A. Surface preparation and analysis

The measurements are performed in a PHI ESCA 5600 XPS system equipped with an additional preparation chamber. Both vacuum systems are connected via an UHV valve to allow for sample transfer without air contact. The analysis chamber has both a standard (Mg and Al $K\alpha$) and a monochromatic (Al $K\alpha$, $h\nu$=1486.6 eV) x-ray source. It is equipped with an ion gun (Specs IQE 12/38) and provides a

base pressure better than 2×10^{-8} Pa. Using the monochromatic x-ray source a resolution of 0.26 eV is achieved in XPS spectra. The analysis spot is 0.8 mm in diameter. We calibrate the binding energy by measuring gold (Au $4f_{7/2}$: 84.00 eV), silver (Ag $3d_{5/2}$: 368.3 eV), and copper (Cu $2p_{3/2}$: 932.7 eV) peaks.[22] All binding energies given in this paper are referenced to the Au $4f_{7/2}$ peak position.

The preparation chamber (base pressure better than 2×10^{-8} Pa) contains a commercial evaporation source (Omicron EFM3) operated with additional power supplies for carbon deposition. The carbon layers are deposited from the vapor phase by electron beam evaporation from a graphite rod (Goodfellow, 99.999%). During the deposition procedure the substrates are held at RT (pressure better than 3×10^{-7} Pa). A quadrupole mass spectrometer is used for residual gas analysis.

Carbon films are deposited on Ni and Fe single crystal substrates. The Ni (1 cm in diameter) and Fe crystals (0.5 cm in diameter) are used after mirror-finish polishing. We use the Ni(111), Ni(100), and Fe(110) surface orientations as examples for surface atom densities from dense to open surface atom packings [surface atom density: Ni(111)>Fe(110)>Ni(100)]. The substrates are cleaned by sputtering (3 kV Ar^+) and annealing (970 K) cycles until no impurities are detected in the XPS spectra. After surface preparation the carbon films are deposited with film thicknesses up to several nanometers followed by XPS analysis. The pass energy of the XPS system is set to 93.90 eV for survey scans and 2.95 eV for high resolution spectra in order to deconvolute components in the C 1*s* binding energy regions. X-ray source and analyzer entrance axis are arranged at an angle of 90°. To achieve highest signal intensity with best information rate originating from the interface region, we orient the sample to a takeoff angle of 22° with respect to the surface normal. After the carbon film characterization at RT (~300 K) the samples are annealed in two experimental procedures (denoted as A and B in this paper). During procedure A, the samples are annealed in steps of 50–100 K up to 970 K by holding the sample at each temperature for 30 min. After cooling down to RT the samples are analyzed again with survey and high resolution scans. This procedure A allows us to analyze the chemical phases that are accessed by the respective annealing temperatures. Details are given in a separate publication.[28] In order to determine kinetic parameters we use procedure B. In this experimental strategy samples are held at different elevated temperatures for several hours. The samples are analyzed while annealing using survey and high resolution scans (only C 1*s* signal) alternatingly. The survey scans are used for thickness (carbon amount) evaluation, while the high resolution scans enable the deconvolution of the C 1*s* signals and from this a determination of kinetic parameters for the occurring reactions. The determination of carbon film thicknesses uses both the carbon and substrate signals and is described elsewhere in detail.[28] The C 1*s* signals are analyzed using a commercial software package [MULTIPAK (Ref. 23)]. For the fit procedure of the components within the C 1*s* signal, we apply Gauss–Lorentz lineshapes and use a Shirley-type background. The metal signals are not analyzed in detail.

B. DFT calculations

The calculations on carbon diffusion were performed with SEQQUEST,[24,25] a periodic DFT program with localized basis sets. As exchange-correlation functional we used the PBE generalized gradient approximation.[26] While the core electrons of each metal atom were replaced by an optimized, norm-conserving pseudopotential,[27] the remaining valence electrons were treated explicitly with a contracted double zeta plus polarization basis set of Gaussian functions, which had been optimized for the atom and solid. Throughout the studies we used a Brillouin zone sampling of 10×10 *k* points for the corresponding 1×1 surface unit cells, which had been carefully checked for convergence.

All calculations were performed with a six-layer slab, where the last two layers were fixed to their calculated bulk crystal structures, while the remaining four layers plus the carbon atom (except the direction of diffusion) were fully optimized (to <0.01 eV/Å). Due to the dipole correction employed in SEQQUEST, the diffusion was explored on one side of the slab only. The process itself was studied with a 2×2 surface unit cell, resulting in 0.25 ML coverage, by successively pushing the carbon atoms into the surface and reoptimizing the system in each step. Due to the low number of degrees of freedom, we found this procedure to be more appropriate than using transition state finding methods.

III. RESULTS AND DISCUSSION

A. Carbon films after RT deposition and annealing experiments, applying procedure A

A detailed characterization of carbon films on Ni(111), Ni(100), and Fe(110), both after RT deposition and after annealing applying procedure A (including the description of their interactions with the substrates), is presented elsewhere.[21,28] Here, we give a brief summary. Although the Ni_3C and Fe_3C formation reactions from the elements are endothermic, a small carbide intensity after RT deposition on the metal substrates (Fe and Ni) is observed. The RT reactivity is higher on Fe(110) compared to the two Ni substrates, Ni(111) and Ni(100), which show similar reactivities. The carbide intensity is restricted to the carbon-metal interface and amounts to 1 ML at maximum. Signatures of the carbide formation are found in the layer (C 1*s*) and substrate (Ni $2p_{3/2}$, Fe $2p_{3/2}$) signals, respectively, as well as the valence band region. The carbide intensity is observed in the C 1*s* signal as binding energy shifts of −0.7 eV (Ni_3C) and −0.8 eV (Fe_3C), compared to the graphite peak position at 284.2 eV. Both metal signals, as well as the intensity maximum in the valence band region, show a small shift toward higher values ($\Delta BE=+0.2$ eV). The C 1*s* signals are dominated by the elemental signals, besides which a small carbide peak is observed. This elemental (not reacted) carbon consists of a graphitic and a disordered graphitic fraction. The latter component is observed at 285.1 eV ($\Delta BE=+0.9$ eV). This peak component is assigned to a disordered graphitic structure since its intensity increases with ion bombardment (e.g., Ar^+) and decreases during annealing treatments. For a detailed description we refer to Ref. 17.

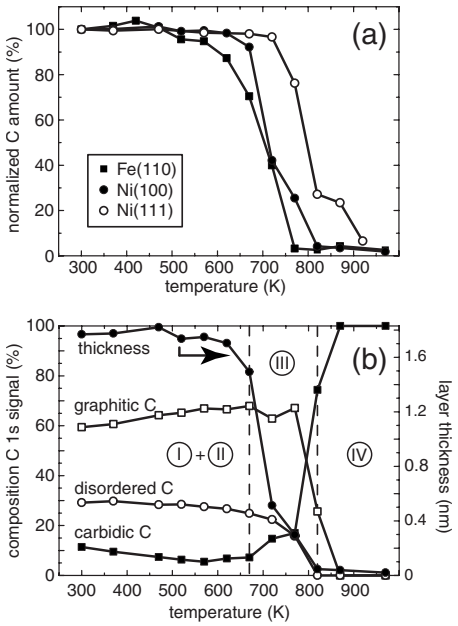

FIG. 1. Normalized carbon amount of carbon films on Fe(110) (■), Ni(100) (●), and Ni(111) (◯) in (a) after annealing steps according to experimental procedure A (see text). The carbon diffusion sets in at 620, 670, and 770 K, respectively. Within a temperature range of 150 K the carbon is almost completely lost into the metal bulk on all three surfaces. The C 1*s* signal composition of a 1.8 nm carbon layer on Ni(100) with increasing annealing temperature is plotted in (b). Up to 570 K carbide decomposition [reaction (I)] is visible. The ordering reaction [reaction (II)] is observed up to 670 K. The carbon diffusion [reaction (III)] sets in at 670 K, accompanied by carbon loss into bulk material and increasing carbide intensity (carbide formation reaction). After the pronounced carbon diffusion the remaining carbon signal is caused by carbon segregation [reaction (IV)].

The thermal behavior applying procedure A is illustrated in Fig. 1. In panel (a) carbon films on all three metal surfaces investigated in this study are compared. The carbon amounts are normalized to the value after RT deposition (300 K). In Fig. 1(a) the onset of carbon diffusion is visible as a loss of carbon from the near-surface region into the metal bulk and therefore out of the XPS information depth (the amount drops below 94% of the initial value). On Fe(110) the carbon diffusion sets in at 620 K, followed by Ni(100) at 670 K and Ni(111) at 770 K. The onset temperature corresponds to the tendency of the activation barriers for carbon bulk diffusion given in literature, as summarized in Table II.[1] Furthermore, the trend in the onset temperature reflects the surface atom densities in the series $(100)<(111)$ for the two nickel surfaces. In Fig. 1(b) the details of the temperature evolution in the carbon layer thickness and the C 1*s* details are shown for a carbon film on Ni(100) with an initial thickness of 1.8 nm. The evolution of the carbon layer thickness is equivalent to the normalized curve in Fig. 1(a). As described above, carbidic and elemental carbon species are identified within the C 1*s* signal. The latter carbon component consists of the graphitic and disordered graphitic fractions. The evolution with annealing temperature of the carbon species in the different chemical environments indicates three regions of different chemical reactions. These temperature regions and the reactions within are labeled by (I)–(IV). Reaction (I) describes the decomposition of carbide, indicated by the carbide signal intensity decrease up to 570 K. Since the carbon layer thickness is unaffected and therefore carbon subsurface or bulk diffusion can be excluded in this temperature region, we refer this behavior to a carbide decomposition reaction. The carbide decomposition is also observed on Fe(110) and Ni(111) and is explained by the metastable character of the respective surface carbides, which are created during the carbon layer deposition at RT. Parallel to the carbide decomposition reaction (I), we identify an ordering reaction (II) within the elemental carbon signals. This reaction is observed on all substrates investigated by now (Au, W, Ti, Si, Be, Fe, and Ni).[14–16,21] The ordering reaction leads to a decrease of the disordered graphitic carbon intensity and is observed until carbon diffusion through the interface into the bulk substrate (reaction III) sets in. While the total carbon signal decreases (due to carbon bulk diffusion), the relative intensity of the carbide signal increases. We assign this relative increase to the carbide formation reaction, producing additional carbide in the surface zone. As mentioned above, the respective carbides are intercalation compounds with carbon atoms in sites within the metal lattice. Therefore, carbon diffusion is required for carbide formation. The relative increase in carbide signal intensity depends on the substrate surface. On Fe(110) and Ni(100) we observe after pronounced carbon diffusion only signal intensity originating from carbidic carbon, while on Ni(111) elemental carbon is still detected up to 920 K. Above the onset temperature of the carbon bulk diffusion, the C 1*s* signal intensity is almost completely lost. The remaining carbon amounts to less than 1 ML and is explained by carbon segregation [reaction (IV)] while cooling down to RT from the respective annealing temperature. The remaining C 1*s* signal after the last annealing step at 970 K exhibits only carbidic carbon on Fe and

TABLE II. Activation energies resulting from experimental data (E^{expt}) and DFT calculations (E^{DFT}), as determined in this work, or given in literature (E^{lit}) for carbon diffusion in the bulk metals (E_D), carbide formation (E_C), and graphite ordering reactions (E_O). The precision of E_O is estimated to ±0.2 eV by calculating the model with several energies. For all other experimental energy values the statistical uncertainty is given.

Substrate	E_D^{expt} (eV)	E_D^{DFT} (eV)	$E_{D,\mathrm{bulk}}^{\mathrm{lit}}$ (eV)	$E_{D,\mathrm{bulk}}^{\mathrm{DFT,lit}}$ (eV)	E_C^{expt} (eV)	E_O^{expt} (eV)
Ni(111)	1.9 ± 0.1	1.92	1.5[a,b]	1.62/1.75[c]	1.1 ± 0.4	0.9
Ni(100)	1.4 ± 0.1	1.45	1.5[a,b]	1.62/1.75[c]	1.3 ± 0.2	0.9
Fe(110)	1.3 ± 0.2	1.44	0.8[a]	0.86[d]	1.1 ± 0.2	0.9

[a]Reference 1.
[b]Reference 2.
[c]Reference 5.
[d]Reference 11.

both Ni surfaces. In all experiments carried out according to procedure A, the thermal behavior (i.e., the characteristic onset temperature for the identified reactions) of the thin carbon films depends only on the substrate species and surface structure, and not on the initially deposited carbon layer thickness (investigated up to several nanometers).

From the annealing experiments according to procedure A, we conclude the identification of reactions (I)–(IV). The carbide formation reaction and the carbon diffusion take place in the same temperature regime. Therefore, they can only barely be discerned in this experimental strategy (procedure A). Since we are interested in the respective kinetic parameters for these reactions, we continue with annealing experiments according to procedure B.

B. Determination of kinetic parameters, applying procedure B

Carbon films with initial layer thicknesses of several nanometers are deposited on Fe(110), Ni(100), and Ni(111). These samples are then annealed at several elevated temperatures, which are selected according to the results of procedure A experiments. During the long-term annealing the samples are analyzed at the respective elevated temperatures by XPS. As described in Sec. III A, the different reactions are identified within the changes in the C $1s$ signals, whereas the substrate signals (Fe $2p$ and Ni $2p$) provide no additional information on the change of chemical nature. The first analysis step is the determination of the carbon layer thickness after RT deposition, while annealing, and again at RT after each thermal treatment. It is determined from survey spectra (acquisition time ~5 min), using both substrate and layer signal intensities from the same spectrum. We determine the mean free paths for C $1s$ (λ_C^C) and metal photoelectrons (λ_M^C) passing through the carbon layer by using the empirical fit given in Ref. 29. The respective values are $\lambda_{C\ 1s}^{C}=1.494$ nm, $\lambda_{Fe\ 2p_{3/2}}^{C}=1.201$ nm, and $\lambda_{Ni\ 2p_{3/2}}^{C}=1.082$ nm. For a detailed description of the carbon layer thickness determination, we refer to Ref. 28.

Since the carbon signal decrease depends on the carbon loss into the bulk, i.e., the carbon diffusion through the film-bulk interface, we can use the carbon layer thicknesses (determined from survey spectra) for a quantification of this reaction. The evolution of the carbon layer thickness at elevated temperatures provides the kinetic parameter k_D for reaction (III), which is the carbon subsurface diffusion. The correlation between $d_{C\ 1s}$ (total thickness in nanometers) and k_D (in s^{-1}) is given by

$$-\frac{d[d_{C\ 1s}]}{dt}=k_D(T)d_{C\ 1s}\rightarrow \ln\frac{d_{C\ 1s}}{d_{C\ 1s,0}}=-k_D(T)t. \qquad (1)$$

The respective initial conditions are as follows: $d_{C\ 1s}$ is the carbon layer thickness at each time t at temperature T and $d_{C\ 1s,0}$ is the carbon layer thickness at $t=0$ and temperature T. Thereby we assume a first order reaction for carbon diffusion. In Fig. 2 the evolution of $\ln(d_{C\ 1s}/d_{C\ 1s,0})$ with annealing time is plotted for Ni(111), Ni(100), and Fe(110) in (a), (b), and (c), respectively. For the highest temperatures in panels (b) and (c) the assumption of a first order reaction is

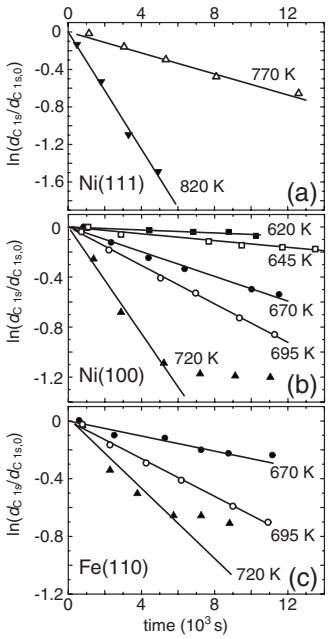

FIG. 2. Determination of $k_D(T)$ using the time-dependent evolution of the carbon layer thickness at different temperatures on Ni(111) in (a), Ni(100) in (b), and Fe(110) in (c). The decrease of the layer thickness is plotted under an assumption of a first order reaction ($\ln[d_{C\ 1s}/d_{C\ 1s,0}]$ vs t).

valid only up to an annealing time of ~6000 s. Above, a deviation from the linear fit is observed. All other values comply with the linear behavior in the logarithmic plot, justifying the first order assumption. Under the assumption of an Arrhenius behavior of $k_D(T)$, we can determine the respective activation barrier for carbon subsurface diffusion (E_D) as given by

$$k_D(T)=k_0\exp\left(-\frac{E_D}{k_BT}\right). \qquad (2)$$

Here, k_0 (in s^{-1}) is the pre-exponential factor, k_B is the Boltzmann constant, and T is the temperature (in Kelvin). The Arrhenius plots in Fig. 3 show the linear behavior of $\ln k(T)$ with T^{-1} for Ni(100) and Fe(110). In the case of Ni(100) and Fe(110), we use for the highest temperatures the data up to 6000 s with a clearly linear relationship between $\ln(d_{C\ 1s}/d_{C\ 1s,0})$ and t (Fig. 2). For Ni(111) only two measurements are available at 770 and 820 K and are used for the determination of E_D. The resulting experimentally determined activation barriers E_D^{expt} for all three surfaces are given in Table II.

During the experiments according to procedure B, alternatingly spectra in survey and high resolution modes are measured. The C $1s$ spectra in high resolution mode (acquisition time 7–10 min) are measured several times consecutively, followed by one survey spectrum for the determination of the carbon layer thickness. For the total C $1s$ signal intensity we use the time evolution of carbon layer thicknesses, which result from the $k_D(T)$ time dependence [Eq. (1)]. As mentioned above, we deconvolute the C $1s$ signal with an elemental (not reacted) and a carbidic carbon fraction. The elemental carbon consists of graphitic and disordered graphitic C. We determine the thicknesses of these fractions within the total C $1s$ signal under the assumption

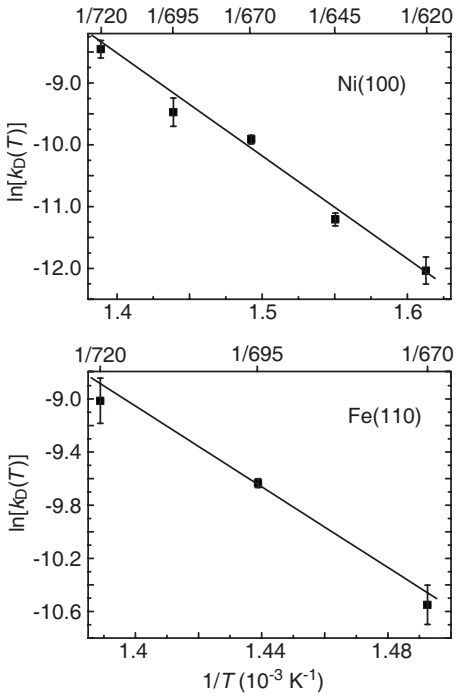

FIG. 3. Determination of the diffusion barrier (E_D) under the assumption of an Arrhenius behavior for Ni(100) and Fe(110) [see Eq. (2)]. The resulting activation barriers are given in Table II.

of equally distributed components in the carbon layer and relate the fraction intensities to the respective thicknesses.

Figure 4 shows a schematic overview of the reactions identified within annealing procedure A, as described above in Sec. III A. These reactions are analyzed in detail with annealing experiments according to procedure B. The determination of the kinetic parameters for reaction (III) (k_D and E_D) are given above. The other reactions are analyzed with the following assumptions and correlations.

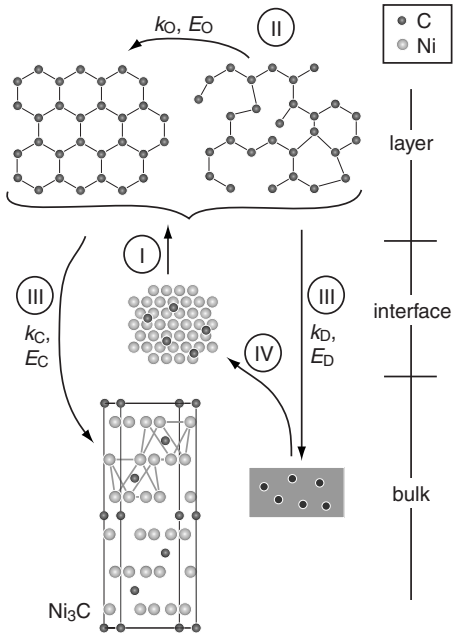

FIG. 4. Illustration of the reactions identified within annealing experiments according to procedure A (see Fig. 1), as an example shown for carbon layers on Ni(111). The respective kinetic parameters for reactions (II), ordering reaction, and (III), carbon subsurface diffusion and carbide formation, are determined by experiments according to annealing procedure B.

- Decomposition of the initially formed carbide [reaction (I)] leads to an increase in elemental carbon, in particular, to an increase of the graphitic component.
- The ordering reaction (II) within the elemental carbon leads to a decrease in disordered graphitic C.
- Carbon subsurface diffusion [reaction (III)] leads to loss in signal intensity of all components of the C 1*s* signal.
- Carbide formation [parallel to reaction (III)] leads to an additional decrease in the elemental carbon intensity.
- Carbon segregation [reaction (IV)] while cooling down to RT leads to an increase in total C 1*s* signal intensity and to an increase of the carbidic signal.

The last process [reaction (IV), carbon segregation] can be neglected because the XPS spectra are measured at elevated temperatures and carbon segregation is only observed while cooling down to RT. Since carbon films are analyzed at elevated temperatures higher than 570 K, also the carbide decomposition reaction (I) can be neglected because it occurs only at temperatures below 570 K. The other reactions (ordering reaction and carbide formation) can be analyzed by XPS measurements using procedure B.

The carbide formation reaction is quantified by analyzing the decrease of elemental carbon and the total C 1*s* signal intensities. Since the carbide formation is accompanied by carbon diffusion, these reactions are correlated as given by

$$\frac{d[d_{\mathrm{carb}}]}{dt} = \frac{d[d_{\mathrm{C\ 1}s}]}{dt} - \frac{d[d_e]}{dt} = k_{\mathrm{C}}(d_{\mathrm{C\ 1}s} - d_e). \tag{3}$$

Here, d_{carb} is the thickness of the carbidic fraction, $d_{\mathrm{C\ 1}s}$ is the total carbon layer thickness, and d_e is the respective elemental carbon layer thickness (all thicknesses are given in nanometers). From this equation k_{C} is determined, which describes the loss of elemental carbon due to carbide formation. Both thicknesses ($d_{\mathrm{C\ 1}s}$ and d_e) are additionally affected by carbon diffusion (k_D). Solving Eq. (3) under consideration of the carbon layer thickness [Eq. (1)] leads to

$$d_e(t) = e^{(k_{\mathrm{C}}t)}[d_{e,0} + d_{\mathrm{C\ 1}s,0}(-1 + e^{-(k_{\mathrm{C}}+k_D)t})]. \tag{4}$$

Using the time-dependent evolution of d_e with the initial conditions ($d_{\mathrm{C\ 1}s}|_{t=0} = d_{\mathrm{C\ 1}s,0}$ and $d_e|_{t=0} = d_{e,0}$), the k_{C} values at the annealing temperatures T are determined. Figure 5 shows the decrease of normalized d_e with annealing time t on Ni(111) in (a), Ni(100) in (b), and Fe(110) in (c). The lines in the plots result from Eq. (4), using the determined $k_{\mathrm{C}}(T)$ and $k_D(T)$ values. Assuming again an Arrhenius behavior, E_{C} is determined as described in Eq. (2). The resulting values are given in Table II.

Similar to the approach described before, the ordering reaction is analyzed using the respective interdependent car-

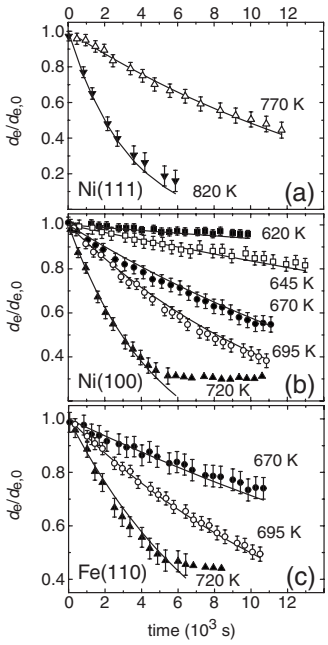

FIG. 5. Determination of $k_C(T)$ using the decrease of elemental carbon at different temperatures on Ni(111) in (a), Ni(100) in (b), and Fe(110) in (c). The lines given in the panels are evaluated using Eq. (4). The resulting activation barriers (E_C) are given in Table II.

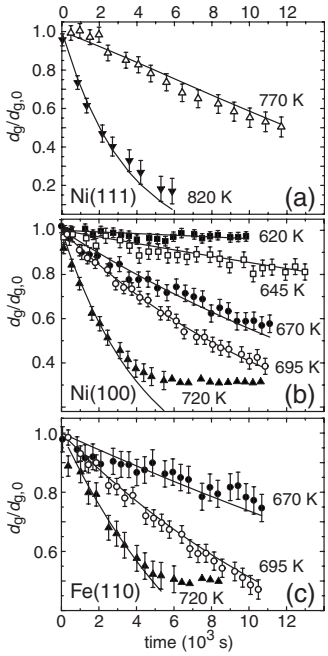

FIG. 6. Decrease of graphitic carbon at different temperatures on Ni(111) in (a), Ni(100) in (b), and Fe(110) in (c). The lines result from Eq. (6) using the described assumptions for the ordering reaction within the elemental carbon. The activation barriers (E_O) are given in Table II.

bon fractions and k values. In a first step the evolution of the disordered graphitic fraction within the elemental carbon signal d_{dis} is defined, as given by

$$\frac{d[d_{\mathrm{dis}}]}{dt} = \frac{d[d_e]}{dt} - \frac{d[d_g]}{dt} = -k_O(d_e - d_g). \tag{5}$$

The respective parameters are the thicknesses of graphitic carbon (d_g), total elemental carbon (d_e), and k_O, the kinetic parameter for the ordering reaction. Moreover, the correlation between d_e and $d_{\mathrm{C\ 1}s}$ has to be accounted for. Both the graphitic carbon and the disordered fraction are affected by carbon subsurface diffusion (k_D) and carbide formation (k_C). Therefore, the graphitic fraction increases by the ordering reaction but decreases with carbon diffusion and carbide formation. Solving Eq. (5) by using these conditions leads to

$$d_g(t) = e^{-(k_O t)}[d_{g,0} + d_{e,0}(-1 + e^{(k_C + k_O)t}) + d_{\mathrm{C\ 1}s,0}(-e^{(k_C+k_O)t} + e^{(-k_D+k_O)t})]. \tag{6}$$

The initial conditions are as mentioned above: $d_{\mathrm{C\ 1}s}|_{t=0} = d_{\mathrm{C\ 1}s,0}$, $d_e|_{t=0} = d_{e,0}$, and $d_g|_{t=0} = d_{g,0}$. This equation includes all kinetic parameters (k_D, k_C, and k_O). Figure 6 shows the decrease in graphitic carbon ($d_g/d_{g,0}$) with annealing time t of carbon films on Ni(111) in (a), Ni(100) in (b), and Fe(110) in (c). The lines represent the values resulting from Eq. (6), which lead, again under an assumption of an Arrhenius behavior [Eq. (2)], to the respective E_O values. Since the ordering reaction is a process within the carbon layer, it should be independent of the substrate and should give the same E_O values for all substrates. As summarized in Table II, the activation barriers are identical within the experimental precision for the three substrate surfaces, confirming the confinement of the ordering reaction to the carbon layer.

The carbide decomposition reaction and carbon segregation are not determined by XPS measurements using procedure B. All other reactions are analyzed with the described assumptions. Section III C presents calculations using the DFT in order to verify the resulting kinetic parameters.

C. DFT calculations

In order to simulate the process of carbon diffusion from the surface into the material on the three surfaces of this work, each study is started with initially optimizing a carbon adsorbate layer. After this preoptimization the adsorbates are successively pushed into the surface and the energy is mapped. Since diffusion into the surface induces certain strain to the surface atoms, a coverage of 0.25 ML (2×2 surface unit cell) is assumed, giving enough freedom to the surface atoms. To ensure that the system is (almost) not constrained by the simultaneous diffusion of the periodic images, we also performed similar calculations with finite clusters, finding the same behavior.

First, the diffusion of carbon into Ni surfaces is studied, which have either (111) or (100) orientation. Starting with the hexagonal close packed (111) surface plane, where carbon preferentially adsorbs on fcc sites and forms three equivalent C–Ni bonds with $a(\mathrm{C-Ni}) = 1.83$ Å, we observe that during the diffusion carbon pulls one of the nearby Ni atoms (see Ni_1 in Fig. 7) out of the surface plane by almost 0.7 Å. Through the thus opened "hole", the carbon atom migrates to octahedral subsurface sites, with an effective energy barrier of 1.92 eV, which nicely compares to the experimentally determined E_D of 1.9 eV. Since the vacant octahedron offers enough space for the carbon, after this *out-of-plane* process Ni_1 equilibrates back to the surface layer. By diffusing into the surface the system gains an overall energy

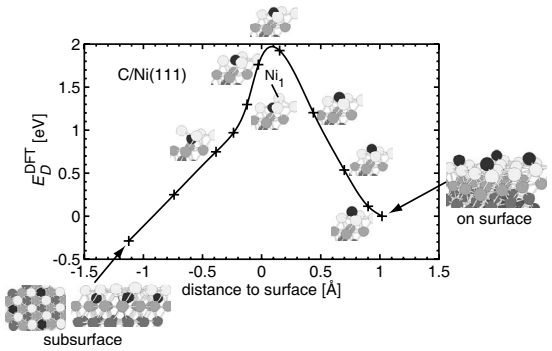

FIG. 7. Theoretical activation energy E_D^{DFT} as a function of the distance of carbon to the surface layer for Ni(111) (referenced to the adsorbed system). The curve is obtained by overlapping the curves for diffusion into the surface and afterward diffusion back onto the surface. While for the initial (surface) and final (subsurface) structures an extended system is shown, the process itself is sketched with figures of various intermediate structures with a 2×2 unit cell only. The process shown here is comparable to the C diffusion into Fe(110). (Lines to guide the eyes.)

of 0.29 eV per C atom. In order to further manifest the transition state, the process and energy barrier are afterward verified by calculations modeling the reverse diffusion back to the surface.

Carbon diffusion into the Ni(100) plane was investigated in an analogous way (see Fig. 8). In contrast to Ni(111), where at the fcc site there is no Ni atom below in the second layer, in the case of Ni(100) the direct vertical diffusion is hindered by a second Ni atom below. Consequently, the vertical migration is accompanied by a horizontal diffusion, by which again one Ni atom (Ni_1 in Fig. 8) is pushed out of the surface layer by 1.1 Å, finally allowing carbon to occupy a nearby bipyramidal subsurface site. The energetic barrier is calculated to be 1.45 eV, which is in very good agreement with the measured value of 1.4 eV. This value is again verified by checking the reverse process. Since Ni(100) is a relatively open surface compared to Ni(111), the calculated and measured diffusion barriers are in much better correspondence to the energetic barrier for bulk diffusion. Similar to Ni(111) it is found that having carbon in subsurface positions is 0.31 eV per carbon more stable than adsorbed on the surface.

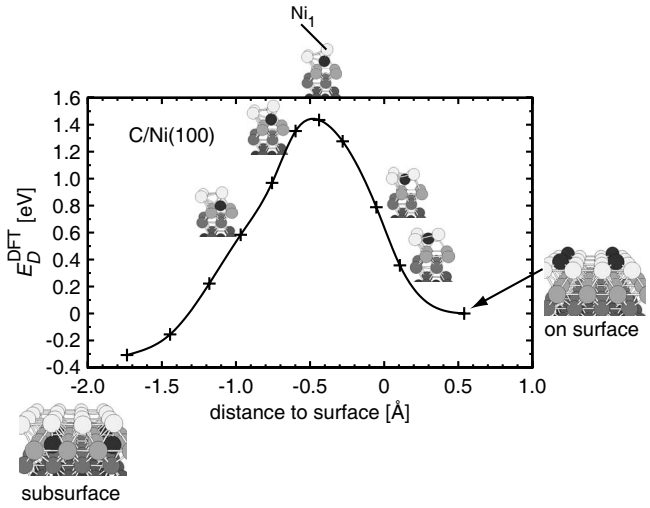

FIG. 8. Theoretical activation energy E_D^{DFT} as a function of the distance of carbon to the surface layer for Ni(100) (referenced to the adsorbed system). The curve is obtained by overlapping the curves for diffusion into the surface and afterward diffusion back onto the surface. While for the initial (surface) and final (subsurface) structures an extended system is shown, the process itself is sketched with figures of various intermediate structures with a 2×2 unit cell only. (Lines to guide the eyes.)

Finally, the carbon subsurface diffusion step into Fe(110) is studied and a similar out-of-plane process is discovered, as already described for Ni(111). Therefore, only the obtained diffusion barrier of $E_D^{DFT}=1.44$ eV is reported. Motivated by the experiment, further studies will aim at investigating the carbide formation process.

D. Discussion

The reactions identified within the experimental procedure A are analyzed in detail by annealing carbon films at elevated temperatures for several hours (procedure B). The C 1*s* signal intensity corresponds to the total carbon layer thickness. Analyzing the evolution of this intensity with annealing time at different temperatures provides the quantification of carbon diffusion into the metal substrate. A first, more qualitative assumption concerning carbon diffusion results from the onset temperature in procedure A (see Sec. III A). In accordance with the tendency of the respective literature bulk diffusion values, an earlier onset on Fe(110) compared to Ni is observed. The two Ni surfaces also differ in their onset temperature for carbon diffusion. As expected, the more open surface structure of Ni(100) shows a lower diffusion onset temperature compared to Ni(111), representing the most dense surface atom packing.

As shown in Sec. III B, the determination of the subsurface diffusion barriers using procedure B for these three surfaces is successful. The decrease of surface carbon amounts corresponds to a first order reaction and the evolution of layer thicknesses with annealing time complies with this. In the case of Ni(100) and Fe(110) we observe a deviation from a first order reaction kinetics only for the highest temperature investigated here (720 K). This observation is explained by the experimental procedure. We deposit thin films on the substrate and lose the carbon through diffusion into the bulk. However, the solubility of carbon atoms in Ni and Fe is small. This is observed in our experiments as carbon segregation while cooling down to RT, already also known from literature.[9,19] The small solubility of C in Fe and Ni was already used for surface enrichment experiments and the measurement of bulk to surface diffusion and segregation, respectively, applying AES and low-energy electron diffraction (LEED) analyses.[30–33] Furthermore, this behavior indicates a diffusion reaction comprising of multiple elemental processes that, however, cannot be observed separately in our experiments. For carbon diffusing from the surface into the bulk metal (i.e., reaching an interstitial site in the metal lattice), in a first step the surface barrier has to be overcome in order to occupy subsurface positions. These interstitial positions within the metal lattice are energetically separated by an energy barrier that describes the diffusion of carbon atoms within the bulk. A carbon atom in a subsurface (first "bulk" position below the surface) interstitial site can diffuse

through the lattice if the diffusion barrier energy is available. In our analysis we do not distinguish between these two activation barriers and describe the carbon diffusion from the surface layer into the bulk as one process. The qualitative justification for this description lies in the argument that the activation barrier for surface-subsurface diffusion is larger than for the bulk diffusion. Therefore, if at a given temperature subsurface diffusion is possible, this is also the case for the bulk diffusion steps. The results for the energy barriers for subsurface diffusion from the experimental analysis are in very good agreement with the values determined by DFT analysis describing, in particular, the surface-subsurface diffusion step. This supports the assumption that the energy barrier for subsurface diffusion is larger than the energy barrier for carbon diffusion within the equivalent bulk sites. Comparing the two nickel surfaces, the activation energies determined in this work (both experimentally and calculated by DFT) are larger for the close-packed Ni(111) surface than for the more open Ni(100) surface. For Ni(100), subsurface diffusion and diffusion within the bulk have very similar values (1.4 eV in our experiment, 1.45 eV in our calculation, and 1.5 eV in literature[2]). For Ni(111), the subsurface diffusion activation barriers are (both experimentally determined and from DFT) 1.9 eV, compared to the bulk literature value of 1.5 eV.[2] This demonstrates that the open surface structure minimizes the additional energy barrier for the subsurface diffusion. Finally, migration of carbon through a carbide and a carbon-rich region with proceeding reactions, respectively, might also influence the activation barriers for diffusion. The latter point could also cause a deviation from a first order reaction.

The components within the C 1*s* signal, which represent the different carbon phases present, are affected by several reactions. These reactions are interdependent and the respective kinetic parameters are determined considering these interdependencies. The carbon diffusion is observed as a decrease of the overall C 1*s* signal intensity. All other reactions observed during the annealing procedure are accompanied by the carbon diffusion and the respective kinetic parameter, k_D, has to be taken into account for the determination of all other parameters. The changes in the elemental carbon intensity is, e.g., affected by the carbon diffusion and by the carbide formation reaction. If carbide formation takes place, we expect a stronger decrease in the total carbon intensity than if caused exclusively by carbon diffusion. Indeed, the decrease proceeds faster than reproduced only by the kinetic parameter k_D. This additional decrease is described by k_C, the kinetic parameter for the carbide formation reaction. As mentioned above, the carbide structures for both nickel and iron are different than a pure carbon intercalation in the metal host lattice. Both metal lattices rearrange for carbon atom incorporation upon carbide formation. The carbon migration into the metal lattices is described by carbon diffusion (k_D). The carbon incorporation in sites within the rearranged metal lattice is characterized by carbide formation (k_C). Since the bulk structure of the carbides is independent of the surface under investigation, we expect similar E_C values for Ni(111) and Ni(100). These values (1.1 and 1.3 eV) agree fairly well within the experimental resolution and confirm the assumptions given above. Furthermore, we expect a similar value for Fe(110) and the Fe_3C formation reaction due to comparable processes within the metal lattice and the carbide structure. The estimated activation barrier for carbide formation in Fe (1.1 eV) is identical to the Ni(111) value. DFT calculations for the carbide formation reaction are not available by now.

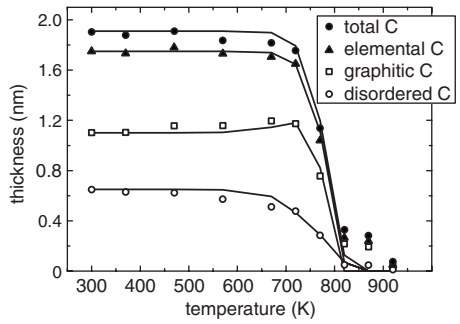

FIG. 9. Experimental results (data points) and simulation (lines) of the thermally induced processes for an initially 1.9 nm carbon film on a Ni(111) surface. The simulation is based on the kinetic parameters for the elemental reactions determined in this work. The experiment is conducted according to procedure A.

The next process that is quantified is the ordering reaction observed within the elemental carbon signal. As mentioned above, the sum intensity decreases due to carbon diffusion. The disordered graphitic fraction decreases further due to the ordering reaction. The carbide formation reaction leads to a decrease of both graphitic and disordered graphitic carbon intensities. Since the ordering reaction is not affected by the substrate, we expect identical parameters for these three surfaces. The resulting activation barriers confirm this. Carbon films on all surfaces investigated here show the same activation barrier (0.9 eV). Literature data or calculated values are not available. The determined kinetic parameters for the elemental reaction steps can finally be used to model the temperature dependent development of carbon films on the investigated substrates. The results of such a model calculation are shown in Fig. 9. The data points represent the experimentally determined carbon species applying procedure A. After each temperature step the sample reaches RT for surface analysis using XPS survey scans (for film thickness determination) and high resolution scans of the C 1*s* core level. Since each temperature step is reached after a short ramp-up time and the sample is cooled down to RT without active cooling, the kinetic values ($k(T)$) and the annealing time have to be corrected by a pre-exponential factor c. Its value, $c=3.5$, scales the annealing time (t) and $k(T)$, as shown by

$$d_x(T_i) = d_x(T_{i-1})\exp^{-ck(T_i)t}. \tag{7}$$

The lines given in Fig. 9 are the results from a simulation using the kinetic parameters for the elemental reactions such as carbon subsurface diffusion (k_D), carbide formation (k_C), and ordering of disordered carbon (k_O). The simulation reproduces the temperature-induced ordering and diffusion processes quantitatively, confirming the model and the respective kinetic parameters developed in this work.

IV. SUMMARY

We present XPS measurements of thin carbon films on Fe(110) and Ni(100) and (111) surfaces for a quantitative deconvolution of different reactions observed during annealing experiments. We determine the kinetic parameters for these reactions, which are interdependent. The substrate element as well as the surface structure affect the carbon diffusion and we determine different activation barriers for these metal surfaces. The calculated values of activation energies for the elemental reaction steps using the DFT approach are in very good agreement with our experimental results. Both experimental and theoretical results confirm the influence of the surface structure, and the resulting values differ from bulk data given in literature. Isothermal annealing experiments allow the determination of kinetic parameters for the observed interdependent reactions (carbide formation and ordering reaction), which facilitate a quantitative description of the thermally induced reactions of carbon films on the investigated surfaces.

ACKNOWLEDGMENTS

T.J. gratefully acknowledges support by the "Fonds der Chemischen Industrie" (FCI) and the "Deutsche Forschungsgemeinschaft" (DFG) within the Emmy-Noether-Program.

[1] H. Bakker, H. P. Bonzel, C. M. Bruff, M. A. Dayananda, W. Gust, J. Horváth, I. Kaur, G. V. Kidson, A. D. Le Claire, H. Mehrer, G. E. Murch, G. Neumann, N. Stolica, and N. A. Stolwijk, in *Diffusion in Solid Metals and Alloys*, Landolt-Börnstein Numerical Data and Functional Relationships in Science and Technology, New Series, Group III: Crystal and Solid State Physics, Vol. 26, edited by H. Mehrer (Springer-Verlag, Berlin, 1990).
[2] S. Diamond and C. Wert, Trans. Metall. Soc. AIME **239**, 705 (1967).
[3] T. A. Massaro and E. E. Petersen, J. Appl. Phys. **42**, 5534 (1971).
[4] B. S. Berry, J. Appl. Phys. **44**, 3792 (1973).
[5] D. J. Siegel and J. C. Hamilton, Phys. Rev. B **68**, 094105 (2003).
[6] F. C. Schouten, E. T. E. Brake, O. L. J. Gijzeman, and G. A. Bootsma, Surf. Sci. **74**, 1 (1978).
[7] F. C. Schouten, O. L. J. Gijzeman, and G. A. Bootsma, Surf. Sci. **87**, 1 (1979).
[8] R. Sau and J. B. Hudson, J. Vac. Sci. Technol. **16**, 1554 (1979).
[9] T. B. Massalski, H. Okamoto, P. R. Subramanian, and L. Kacprzak, *Binary Alloy Phase Diagrams, Version 1.0*, 2nd ed., (ASM International, Materials Park, OH, 1996).
[10] R. B. McLellan and M. L. Wacz, J. Phys. Chem. Solids **54**, 583 (1993).
[11] D. E. Jiang and E. A. Carter, Phys. Rev. B **67**, 214103 (2003).
[12] H. H. Hwu, B. Fruhberger, and J. G. Chen, J. Catal. **221**, 170 (2004).
[13] H. H. Hwu and J. G. Chen, Chem. Rev. (Washington, D.C.) **105**, 185 (2005).
[14] P. Goldstrass, K. U. Klages, and Ch. Linsmeier, J. Nucl. Mater. **290–293**, 76 (2001).
[15] J. Luthin and Ch. Linsmeier, Surf. Sci. **454–456**, 78 (2000).
[16] Ch. Linsmeier, J. Luthin, and P. Goldstrass, J. Nucl. Mater. **290–293**, 25 (2001).
[17] J. Luthin and Ch. Linsmeier, Phys. Scr. **T91**, T134 (2001).
[18] I. Barin, *Thermochemical Data of Pure Substances*, 3rd ed. (VCH, Weinheim, 1995), Vols. 1 and 2.
[19] A. F. Holleman, and E. Wiberg, *Lehrbuch der Anorganischen Chemie* (Walter de Gruyter, Berlin, 1995), 101st ed.
[20] Inorganic Crystal Structure Database, Version 1.2.0, 2003.
[21] A. Wiltner and Ch. Linsmeier, Phys. Status Solidi A **201**, 881 (2004).
[22] M. P. Seah, I. S. Gilmore, and G. Beamson, Surf. Interface Anal. **26**, 642 (1998).
[23] MULTIPAK, Version 6.1A, Physical Electronics, 1999.
[24] P. A. Schultz (unpublished); A description of the method is in P. J. Feibelman, Phys. Rev. B **35**, 2626 (1987).
[25] C. Verdozzi, P. A. Schultz, R. Wu, A. H. Edwards, and N. Kioussis, Phys. Rev. B **66**, 125408 (2002).
[26] J. P. Perdew, K. Burke, and M. Ernzerhof, Phys. Rev. Lett. **77**, 3865 (1996).
[27] D. R. Hamann, Phys. Rev. B **40**, 2980 (1989).
[28] A. Wiltner and Ch. Linsmeier, "Thermally induced reaction and diffusion of carbon files on Ni(111) and Ni(100)," Surf. Sci. (submitted).
[29] M. P. Seah and W. A. Dench, Surf. Interface Anal. **1**, 2 (1979).
[30] M. Eizenberg and J. M. Blakely, Surf. Sci. **82**, 228 (1979).
[31] J. F. Mojica and L. L. Levenson, Surf. Sci. **59**, 447 (1976).
[32] H. J. Grabke, W. Paulitschke, G. Tauber, and H. Viefhaus, Surf. Sci. **63**, 377 (1977).
[33] W. Arabczyk and U. Narkiewicz, Surf. Sci. **352–354**, 223 (1996).